Berreman effect applied to phase characterization of thin films supported on metallic substrates: The case of TiO_2

B. C. Trasferetti and C. U. Davanzo*
Instituto de Química, Universidade Estadual de Campinas, Caixa Postal 6154, CEP-13.083-970 Campinas, São Paulo, Brazil

R. A. Zoppi
Instituto de Ciências Biólgicas e Química, Pontíficia Universidade Católica de Campinas, Caixa Postal 1111, CEP-13020-904 Campinas, São Paulo, Brazil

N. C. da Cruz and M. A. B. de Moraes
Instituto de Física, "Gleb Wataghin," Universidade Estadual de Campinas, Caixa Postal 6165, CEP-13.083-970 Campinas, São Paulo, Brazil

(Received 23 August 2000; published 6 September 2001)

Infrared reflection-absorption spectra of TiO_2 thin films deposited by plasma-enhanced chemical vapor deposition onto aluminum and by a sol-gel process onto platinum were obtained using *s*- and *p*-polarized light and oblique incidence angles. Prominent bands with variable reflection minima position and line shapes, which were shown to be phase dependent, were observed for all samples in the $800-900\ cm^{-1}$ wave number range when *p*-polarized light and oblique incidence were used. Such bands were attributed to an LO mode of TiO_2 and their enhancement with the incidence angle is a good example of Berreman effect. Such spectra were analyzed by means of spectral simulation based on the Fresnel equation for a three-layered system. The films' optical constants used in the simulations were obtained through the Kramers-Krönig analysis (KKA) of the reflectance spectra of pellets of powdered amorphous TiO_2, anatase and rutile. Optical constants for hypothetical polycrystalline TiO_2 systems were also calculated from the dielectric functions of single crystals by means of effective medium theories (EMTs), such as those of Bruggeman, Maxwell-Garnett, and Hunderi. These optical constants were used both for spectral simulation and for understanding the bands observed. However, the optical constants for the powdered standards determined through KKA reproduced experimental results more accurately than those determined through the EMTs. In both experimental and simulated spectra, Berreman effect was very clear-cut and a reliable phase characterization could be carried out.

DOI: 10.1103/PhysRevB.64.125404 PACS number(s): 78.20.−e, 33.20.Ea, 87.64.Je

I. INTRODUCTION

Infrared reflection absorption spectroscopy (IRRAS) has been widely applied to characterize the surface and interface of thin films on metallic substrates because of its high sensitivity.[1–3] If *p*-polarized light is used, reflection minima can be observed not only for the transverse optical (TO) excitations, but also for the longitudinal optical (LO) ones, as a result of the finite thickness of the film. Such a phenomenon, which is known among spectroscopists as the Berreman effect[4,5] due to the pioneer works of Berreman,[6] is widely exploited for the characterization of very thin films. Berreman argued that, in crystalline thin films, zone-center (long wavelength) phonons have wave vector **K** perpendicular to the film surface, such that normal-incidence radiation can only interact with TO vibrations, in which the atomic displacements are perpendicular to the direction of periodicity of **K**. On the other hand, the *p*-polarized component of oblique incident radiation has subcomponents parallel and perpendicular to the film surface, which in addition to exciting the TO phonon, can also interact with LO vibrations, in which the atomic displacements are parallel to the wave vector.

As far as the authors are aware, Berreman effect has never before been exploited in phase characterization of materials. Among the techniques currently used for phase characterization, x-ray diffraction (XRD) is the most commonly employed. However, the information it provides about amorphous materials is restricted and, in the case of very thin films, it is difficult and time-consuming to obtain a reliable diffractogram. For the case of TiO_2 coatings, Raman spectroscopy (RS) is also very useful for phase characterization, as shown by a series of articles published by Exarhos and co-workers.[7–10] This technique was reported to be very effective in identifying even trace amounts of anatase in a rutile phase due to a very intense band at $143\ cm^{-1}$, which is attributed to anatase. Our aim in this paper is to show that, by virtue of Berreman effect, reliable IRRAS spectra can be obtained even for amorphous and very thin TiO_2 films. Such spectra allowed to infer about solid-state properties of the deposited films. This was accomplished by means of the LO-TO functions of powdered standard samples of anatase, rutile, and amorphous TiO_2 and by means of spectral simulation. We strongly believe that such an approach can be used in phase characterization of other solids that present polymorphism. However, it is mandatory that the material have a polar character for the LO-TO splitting to be observed. Therefore, covalent compounds, such as most of the organic ones, cannot be investigated by this approach.

In this work, IRRAS was used to characterize TiO_2 films

prepared by two different techniques: plasma-enhanced chemical vapor deposition (PECVD) and a spin-coating sol-gel process. The PECVD films were deposited onto aluminum-coated glass substrates, while the sol-gel ones were deposited onto platinum. The former are very smooth, as shown by profilometric analysis, which makes comparison between simulated and experimental results straightforward, and the latters are rough. For the sol-gel films, platinum was the substrate chosen because these films were prepared with the aim of an electrochemical investigation. It will be shown that, despite platinum's roughness, reliable spectra could be obtained within the low-wave number region and inferences about film phase could be made even without having exact information about film thickness. As with other semiconductor oxides, TiO_2 has been extensively studied due to its photoelectrochemical[11,12] and electrochromic[13,14] properties, whose applications range from photocatalysis to smart windows.

Our study is restricted to the Mid-Infrared wavenumber region because far-infrared reflection-absorption measurements are difficult to be carried out by using conventional sources due to their characteristic low emission. We have observed experimentally intense bands in the $800-900\ \mathrm{cm}^{-1}$ wavenumber range for the three different TiO_2 structures we studied. Although they are expected according to calculations presented in pioneering works[15–17] from the 1960's, this is the first time they are directly observed in an experiment, as far as the authors are concerned.

This paper is organized as follows. In Sec. II we describe both the experimental procedures for making and measuring thin films of TiO_2 and the analytical procedures for obtaining experimental results, such as infrared spectra, field emission scanning electron microscopy (FESEM) micrographs and x-ray diffractograms. In Sec. III A, we discuss LO and TO functions for polycrystalline TiO_2 obtained through well-known effective medium theories (EMTs) and LO and TO functions calculated through the Kramers-Krönig analysis (KKA) of the reflectance spectra of pellets of powdered TiO_2 standards. Section III B is a description of how spectral simulations were carried out. While in Sec. III C we discuss the experimental results for the PECVD films, in Sec. III D we discuss those for the sol-gel films. Conclusions drawn from the infrared study are described in Sec. IV.

II. EXPERIMENTAL

A. PECVD films

The PECVD TiO_2 films were obtained from mixtures of titanium (IV) isopropoxide $[Ti(OC_3H_7)_4]$, from now on called TTIP, with He and Ar using an experimental apparatus described elsewhere.[18] Briefly, it consists of a stainless steel vacuum chamber fitted with two parallel-plate electrodes connected to a 13.56 MHz radiofrequency generator. The substrate holder was positioned outside the electrode gap and at a distance of about 3 cm from the electrode edges. During deposition, a voltage bias could be applied to the substrate, connecting the substrate holder to a dc power supply. The substrate could be also heated by an electrical resistor attached to the substrate holder, whose temperature was measured with a thermocouple. Precision mass flowmeters were used to admit He and Ar (purity better than 99.99%, White Martins) in the chamber, while TTIP (99% pure, Aldrich) was admitted from a heated evaporation cell. The pressure was measured with a capacitance manometer. All depositions were made with He and Ar flows of 3.0 and 5.0 sccm, respectively, and a partial pressure of TTIP of 0.3 Pa.

Several films were deposited onto aluminum-coated glass substrate using different deposition parameters. Film thicknesses were determined using a profilemeter (Veeco, Dektak3). To illustrate the technique presented here, two PECVD films were used: sample P1 and P2. Both were deposited using a substrate bias of $+200$ V. P1 was deposited without heating the substrate during deposition whereas P2 was deposited with the substrate heated up to 300 °C. The substrate used was aluminum evaporated thermally onto a glass slide. The thickness of sample P1 was 0.45 μm and of sample P2 was 0.25 μm.

B. Sol-gel films

The TiO_2 films were deposited using the spin-coating process, with a nonaqueous sol-gel precursor. The precursor used was a solution of 1.20 mL TTIP (Aldrich) diluted in 30 mL of isopropyl alcohol P.A. (Merck). To provide proper conditions for the acidic hydrolysis, 0.1 mL of concentrated HCl (Merck) were added to the precursor solution. The mixture was stirred during 1 h in an open flask at 50 °C. The platinum substrate was placed on a spin-coater (Photoresist Spinner Headway research EC101DT-R485) and spun at 3000 rev min^{-1}. Keeping the sol at 50 °C, a volume of 500 μL was dripped onto the substrate in portions of 100 μL. The substrates used in this work were platinum (99.95%). After deposition, the samples were annealed at four different temperatures (100, 400, 600, and 800 °C) for 1 h and labeled according to them as S100, S400, S600, and S800.

C. Infrared spectra acquisition

Infrared reflection-absorption spectra were measured for all samples in a Bomen MB-101 FT-IR spectrometer equipped with a DTGS detector. The spectral range covered was $400-5000\ \mathrm{cm}^{-1}$. Each spectrum was the result of co-adding 128 scans collected at 4 cm^{-1} resolution, in the external-specular-reflectance mode, by means of a variable-angle attachment (SPECAC), at the incidence angles 30°, 50° and 70° off normal for both *p*- and *s*-polarized radiation. Polarization was provided by the insertion of a grid polarizer (SPECAC) in the optical path. All reflection-absorption measurements were referenced to an aluminum mirror and they were carried out at room temperature.

D. Determination of the optical constants of TiO_2 standards

Infrared specular reflectance spectra were measured for pellets of powdered amorphous TiO_2, anatase (Aldrich) and rutile (Tilbrás) using the above-mentioned conditions except for the incidence angle, which was kept at 10° off normal, and for the radiation, which was not polarized. The complex

refractive index of this material was determined through the Kramers-Krönig analysis (KKA) of these reflectance spectra. KKA requires an extrapolation of the spectrum to zero and infinite frequencies. There are several extrapolation routines that can be used. In our calculations, we used constant reflectivities derived from the first and last points of the measured spectrum file. The software used was developed by us in a MatLab (The Math Works) environment based on previously reported investigations.[19,20] The amorphous TiO_2 used in this work was obtained through the hydrolysis of TTIP in the air, a process which is well described in the literature since it is the basis of the sol-gel deposition. No crystalline structure was observed for this solid by x-ray diffraction.

E. X-rays diffractograms (XRD) and field emission scanning electron microscopy (FESEM) micrographs acquisiton

X-ray diffraction studies were carried out using a Shimadzu XRD6000 x-ray diffraction analyzer with a CuKa source. Images were obtained in a JSM-6340F JEOL field emission scanning microscope, which allows a better resolution compared to conventional scanning electron microscopes. Samples were coated with carbon.

III. RESULTS AND DISCUSSION

A. TO and LO energy-loss functions

TO and LO energy-loss functions, whose maxima correspond to the vibrational modes TO and LO, respectively, can be obtained from the complex dielectric function $\tilde{\epsilon}$[2]:

$$\text{TO function} = \text{Im}(\tilde{\epsilon}) \tag{1}$$

$$\text{LO function} = \text{Im}(-1/\tilde{\epsilon}). \tag{2}$$

The complex dielectric functions of the crystal forms of titanium dioxide, anatase, and rutile, are available in the literature only for single crystals.[21,22] As for amorphous TiO_2, there is no information about its dielectric function. Since both crystalline forms are uniaxial, there are two different $\tilde{\epsilon}$ for each one: one calculated from the specular reflectance spectrum measured with the electric vector of the incident radiation parallel to the crystallographic c axis ($E \| c$) and the other with the electric vector perpendicular to the crystallographic c axis ($E \perp c$).[21,22] The anisotropic $\tilde{\epsilon}$ for anatase and rutile's single crystals were calculated through the following four-parameter dispersion model based on the factorized form of the dielectric functions from parameters made available by Gonzalez and co-workers[21] (for anatase) and Gervais and Piriou[22] (for rutile):

$$\tilde{\epsilon}(\nu) = \epsilon_\infty \prod_n \frac{\nu_{\text{LOn}}^2 - \nu^2 + i\gamma_{\text{LOn}}\nu}{\nu_{\text{TOn}}^2 - \nu^2 + i\gamma_{\text{TOn}}\nu}, \tag{3}$$

where ν_{LO} and ν_{TO} are the resonance frequency related to LO and TO modes, respectively, while γ_{LO} and γ_{TO} are the damping parameters related to LO and TO modes, respectively. However, since both anatase and rutile are anisotropic crystals, these functions cannot be compared directly to our films' because it is likely that they are in fact polycrystalline, i.e., they are composed of small crystalline regions with random orientations. As will be discussed in Sec. III D, the cracks observed in FESEM micrographs seem to corroborate this hypothesis. A possible solution to this problem would be, at first sight, obtaining $\tilde{\epsilon}$ for polycrystalline TiO_2 which can be accomplished by means of effective medium theories. Polycrystalline TiO_2 is represented by the two different orientations of the crystallites.

TABLE I. Effective medium theories (EMTs) and their formulas.

Effective medium theory (EMT)	Formula
Bruggeman	$\tilde{\epsilon}_{\text{eff}} = \tilde{\epsilon}_1 \frac{1 - f + \frac{1}{3} f\alpha}{1 - f - \frac{2}{3} f\alpha}$
Maxwell-Garnett	$\tilde{\epsilon}_{\text{eff}} = \tilde{\epsilon}_1 \frac{1 + \frac{2}{3} f\alpha}{1 - \frac{1}{3} f\alpha}$
Hunderi	$\tilde{\epsilon}_{\text{eff}} = \tilde{\epsilon}_1 \left(\frac{1 + \frac{1}{4} f\alpha}{1 - \frac{1}{4} f\alpha} \right)$

Although it is not a recent problem, the description of properties of composite materials by EMTs has attracted considerable attention lately.[23–26] Numerous expressions of the effective dielectric function $\tilde{\epsilon}_{\text{eff}}$ of varying degrees of detail and complexity have been developed. However, the validity of each expression seems to be still unknown.[20] Our intention here is not an exhaustive study of EMTs' validity, but we focus on the results they generated for our specific problem.

We took three typical expressions for the effective dielectric function, those derived by Bruggeman,[27] Maxwell-Garnett,[28] and Hunderi,[29] which are summarized in Table I. In the equations shown in Table I, $\tilde{\epsilon}_1$ and $\tilde{\epsilon}_2$ are the dielectric functions of the constituents, f denotes the filling factor, i.e., the volume fraction occupied by constituent 2 and α is a term dependent on the particles' geometry. In our calculations, the particles were assumed to be spherical so that α can be written as

$$\alpha = \frac{\tilde{\epsilon}_2 - \tilde{\epsilon}_1}{\tilde{\epsilon}_1 + \frac{1}{3}(\tilde{\epsilon}_2 - \tilde{\epsilon}_1)}, \tag{4}$$

Bruggeman's theory is the most widely discussed in the literature. In this EMT, one regards a typical element of the two-phase material which are embedded in an effective medium, whose properties are to be determined self-consistently.[30] To achieve this one solves for the local field around the element and imposes the condition that the fluctuations of this local field around its effective value should average to zero. Maxwell-Garnett's theory assumes that the Lorentz local-field correlation applies, that the induced polarization of one particle from its neighbors is instantaneous, and that the distances between the particles are

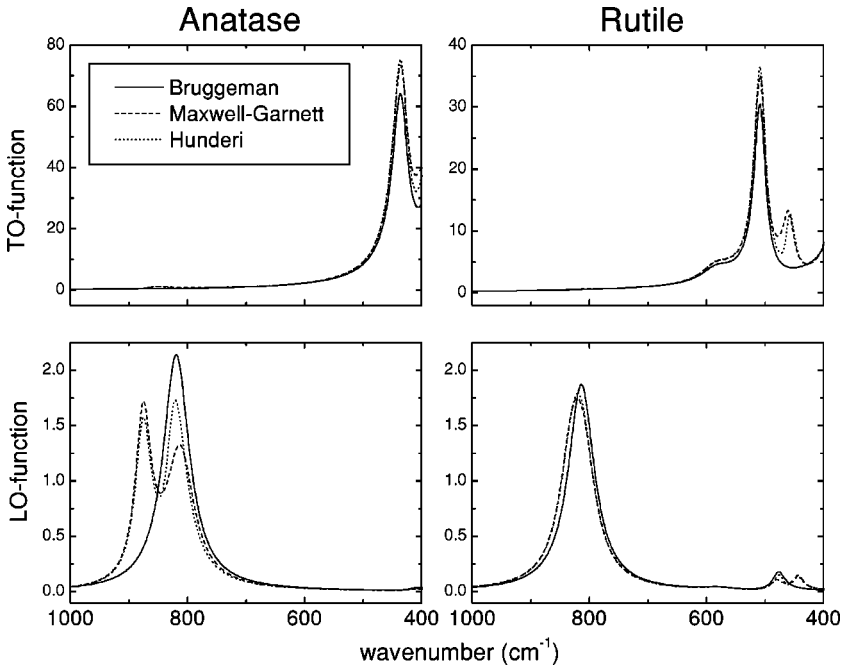

FIG. 1. LO and TO energy-loss functions calculated for polycrystalline TiO_2 by means of EMTs.

so large that they act as independent scatterers.[30] Hunderi's theory was derived from the apparent dielectric function of the backscattered fields.[30]

The results for both rutile and anatase are shown in Fig. 1. Assuming an overall random orientation, the optical properties related to each of the axes contribute equally, and since two (out of three mutually perpendicular) axes are equivalent, the so-called filling factor was set to 0.33 accordingly—we have considered the $\tilde{\epsilon}$ for $E\|c$ as the constituent 2. From inspection of Fig 1, one can easily notice that the EMTs do not yield identical functions. The most striking difference among them is that the functions calculated through the Maxwell-Garnett and Hunderi models presented splittings that were not observed for the functions calculated through Bruggeman's model. Disagreements concerning frequency maxima were also observed.

In order to decide which EMT reproduces the LO and TO functions for polycrystalline TiO_2, we determined LO and TO functions for pressed pellets of powdered TiO_2. Such an approach allows the study of amorphous TiO_2, which is impossible using the methodology discussed above. Since in nonmagnetic materials, $\tilde{\epsilon}$ is related to the complex refractive index through $\tilde{\epsilon}=\tilde{n}^2$, it can be determined from experimental reflectance data by Kramers-Krönig analysis (KKA).[19,20] Such a method has been widely used to determine $\tilde{n}$ of materials in the IR region because it needs only a specular reflectance spectrum observed at some known angle of incidence. A specular reflection spectrum of these powders can be regarded as a superposition of the two polarized single crystal's reflectance spectra attenuated by the fact that the density of the pellet is smaller than that of the single crystal. In this work, KKA was used to determine $\tilde{n}$ of anatase, rutile, and amorphous TiO_2, and subsequently their TO and LO energy-loss functions, which are shown in Fig 2.

Although the physical meaning of TO and LO modes is clear for crystals, the significance of such splittings at atomic level is not totally clear in the case of amorphous materials,[31–37] where the wave vector **K** is not a well-defined quantity. However, using linear response theory, Lehmann[34] has shown that spatial periodicity is not required for the existence of TO and LO surface modes, making their observation also possible in amorphous materials. Since then, several investigations on amorphous materials have been exploiting LO-TO splittings.[31–37] Our results for the amorphous TiO_2 corroborate the possibility of the existence of a LO-TO splitting for amorphous polar compounds. Both TO and LO functions are very broad, which are expected when

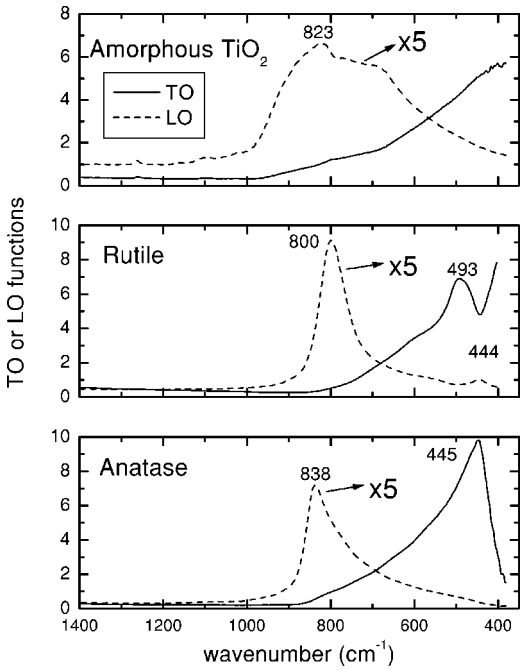

FIG. 2. LO and TO energy-loss functions determined by KKA of the reflectance spectra of pellets of powdered TiO_2 standards.

an amorphous material is concerned. The LO function has a maximum at 823 cm^{-1} with a shoulder in $\sim$ 800 cm^{-1} and has an asymmetric tail in the lower wavenumber region. The TO function probably has a maximum outside the investigated region but displays a tail in the region of higher wave number.

Rutile's LO function has two bands, the most intense one at 800 cm^{-1} and the less intense one at 444 cm^{-1}, while its TO function displays only one band (493 cm^{-1}) in the spectral region investigated. As for anatase, it has a LO maximum at 838 cm^{-1} and a TO maximum at 445 cm^{-1}. Although considerably less pronounced than in the amorphous TiO_2's case, the bands observed for the polycrystalline samples are also asymmetrically broadened, particularly anatase's. Why is it so? The most likely explanation is that the crystal nature of rutile and anatase is anisotropic. In a series of papers,[38–41] Ovchinnikov and Wight investigated inhomogeneous broadening of absorption bands in the infrared spectra of both amorphous and polycrystalline sample. They have shown that the long-range dipole interactions can transcend the grain boundaries in polycrystalline samples having isotropic structures, thereby delocalizing the optical phonon modes over the entire sample and effectively eliminating the dipole broadening.[38] In polycrystalline samples having anisotropic crystal structures, the dipole broadening remains because the unique axes of the individual grains are not aligned in the sample.[38] Therefore, the distribution of frequencies resulting from the various shapes of microcrystalline regions is manifested as inhomogeneous broadening of the band.[38]

Comparing the LO and TO functions calculated from the reflectance spectra of pellets with those calculated by means of EMTs, one can easily notice that the Bruggeman model provides the closest functions to our results for the pellets both in the number of bands and their frequencies. The splittings observed in the functions calculated by the Maxwell-Garnett and Hunderi models were not observed in the functions for the pellets. Spectral simulations carried out using optical constants calculated by the EMTs did not reproduce well the experimental reflection-absorption spectra of the films we have obtained by PECVD, whose thickness we could determinate satisfactorily. Bruggeman's theory led to the best result, but even though it failed to reproduce experimental spectra in a quantitative fashion. As it will be discussed in the next section, the experimental results were well reproduced by simulation carried out using the optical constants determined for the pellets. This may be due to the fact that the pellets are likely to be closer to the structure of our films.

B. Spectral simulations

Figure 3 depicts the incidence of a plane wave in the system studied and introduces the parameters involved in an external reflection measurement for the system consisting of a single film on a semi-infinite substrate. The incident wave is described by the wave number in vacuo ν, the incident angle θ, which is defined relative to the surface normal, and the state of polarization. *s* polarization has the electric vector transverse to the plane of incidence while *p* polarization has it in the plane of incidence. The material parameters are the complex refractive indexes and the thickness *d* of the film. The reflection amplitude for the system of a film layer on a substrate can be written as a function of Fresnel reflection coefficients for each of a three-phase layered system, which has been successfully employed in the modelation of optical properties of multilayered systems. The result of such a procedure is the equation for the reflection amplitude *r* of a three-phase system, which has been described elsewhere.[33] The reflectance *R* of the system is then given by $|r|^2$.

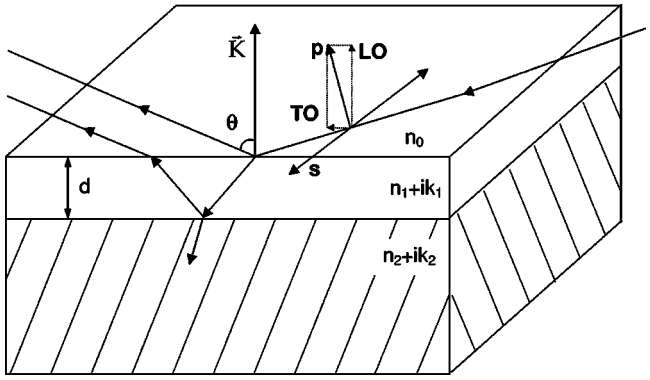

FIG. 3. Parameters involved in an external reflection measurement for the system consisting of a single film on a semi-infinite substrate.

Spectral simulations were carried out for different incidence angles, polarization and thicknesses of an amorphous TiO_2, anatase or rutile thin layer on platinum or on aluminum. The complex refractive indexes of the different TiO_2 phases used in the calculations were the ones determined through the KKA of the reflectance spectra of pellets of the powdered oxides. As for the complex refractive indexes of platinum and aluminum, since they exist in tables[42] and hence are not suitable for computer modelling, their real and imaginary parts had to be fit to polynomials which were functions of the wave number.

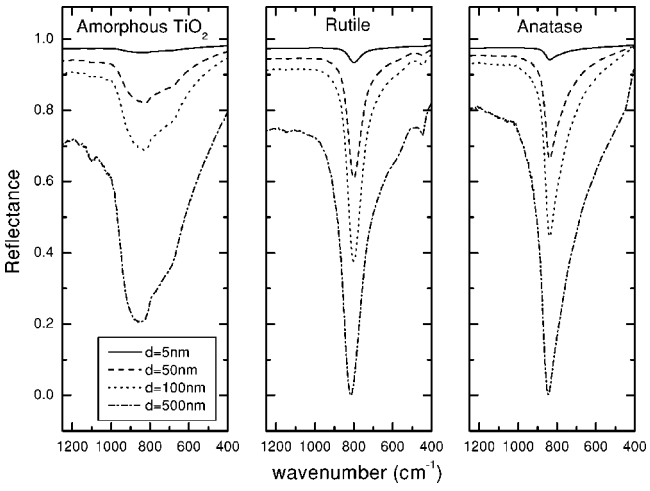

FIG. 4. Simulated reflection-absorption spectra (*p*-polarization and $\theta = 70°$) for a TiO_2/Pt system and four different film thicknesses.

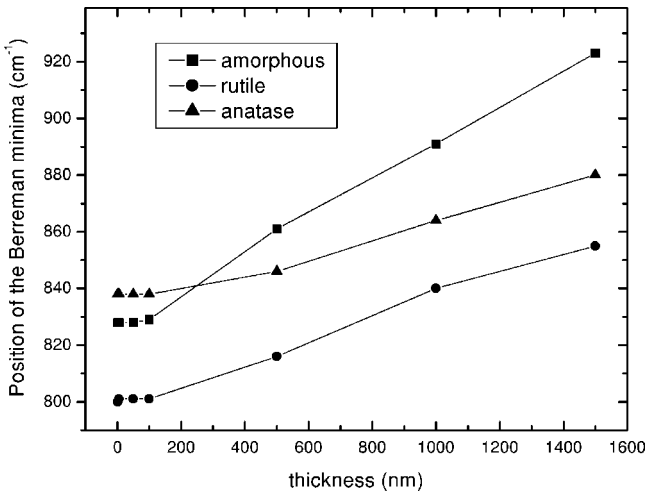

FIG. 5. The effect of film thickness on Berreman minimum for the three TiO_2 phases studied.

Figure 4 shows the spectra simulated using platinum as a substrate, *p* polarization and an incidence angle of 70 °. The films' thicknesses were varied. Within the wave number range presented, the differences between the spectra simulated using the optical constants of platinum and aluminum can be neglected. For thinner films, the simulated spectra reproduces the LO-function features and are not influenced by the TO function. However, as the films get thicker, the spectra begin to be influenced by both functions, but the LO function is still predominant.

A quick glance at Fig. 4 suffices to show that Berreman minimum, i.e., the minimum in reflectance related to an LO mode, is thickness dependent. Such a dependence, illustrated in Fig. 5, does not prevent IRRAS from being used as a phase characterization technique. Amorphous TiO_2 has its characteristic broadened band which cannot be mistaken for one of the crystalline phases. As for the latters, their most intense LO bands lie at different wave number ranges and yet rutile has an LO mode at 444 cm^{-1}, which appears even for very thin films.

C. Experimental spectra: PECVD films

The experimental spectra were obtained for both polarizations and for three different incidence angles. For the *p*-polarized spectra, we have observed a band within the $800-900$ cm^{-1} range, whose intensity increased with incidence angle. Such a band was not observed in the *s*-polarized spectra. Figure 6 shows experimental spectra for samples P1 and P2 that were recorded with $\theta=70$ °. It also shows simulations that were carried out using the optical constants of the amorphous TiO_2 [Fig. 6(a)] and of anatase [Fig. 6(b)], and the films thicknesses determined by a profilometer (450 and 200 nm, respectively).

A good agreement is verified since experimental line shapes are qualitatively reproduced by the simulated spectra. The band observed for sample P2 is narrower than the one observed for P1 and in addition the amorphous TiO_2 band shape is very characteristic. Such a narrowing is often associated to crystallization. The spectrum for P2 was compared

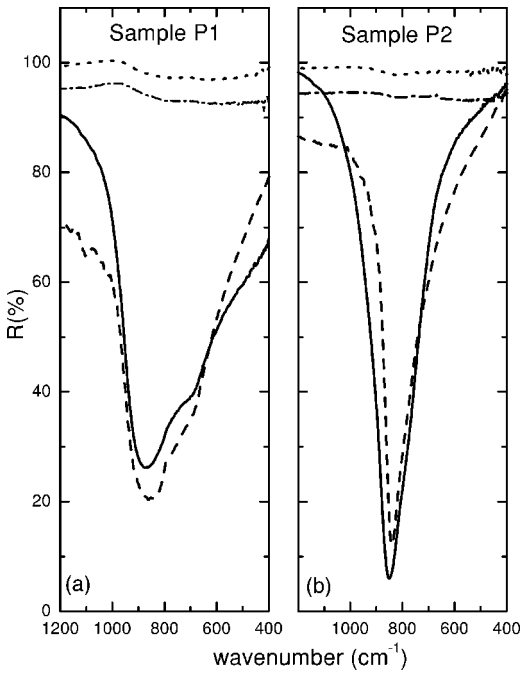

FIG. 6. Experimental spectra for the PECVD films and simulated spectra using the optical constants of amorphous TiO_2 and of anatase. (Solid line) experimental spectra ($\theta=70°$ and *p* polarization); (dashed line) simulated spectra ($\theta=70°$ and *p* polarization); (dotted line) experimental spectra ($\theta=30°$ and *s* polarization) and (dashed dotted line) simulated spectra ($\theta=30°$ and *s* polarization).

with simulations carried out using both anatase and rutile optical constants. However, it was clearly closer to the spectrum simulated for anatase. The Berreman minimum observed lied at 841 and 848 cm^{-1} for the simulated and the experimental spectra, respectively. According to our simulations, such a value is only attainable for rutile if the film thickness is more than 1000 nm. No band at ~ 444 cm^{-1} also excludes the possibility of the film to be rutile. As far as the authors are concerned, this is the first time that these LO bands are detected experimentally.

It is important to remark that, by using XRD, no crystalline structure was observed for sample P1, while a very small peak associated to anatase[43] ($2\theta=25.3°$) was observed for sample P2. No peak associated to rutile was observed.

D. Experimental spectra: Sol-gel films

Figure 7 shows field emission scanning micrographs of the platinum surface which was covered with TiO_2 (S100 and S800). The platinum surface was completely covered by the oxide. However, even for low annealing temperatures, the film surface was not homogeneous and cracks could be observed. As expected, increasing the annealing temperature, the film surface became much more cracked. As a consequence of such inhomogeneity, thickness determination was not possible to be carried out. However, since light scattering increases with the wavenumber, within the range where the TiO_2 LO-bands are observed, the spectrum are not distorted by the above-mentioned cracks and hence, they do not prevent spectral analysis. Figure 5 shows that even when an

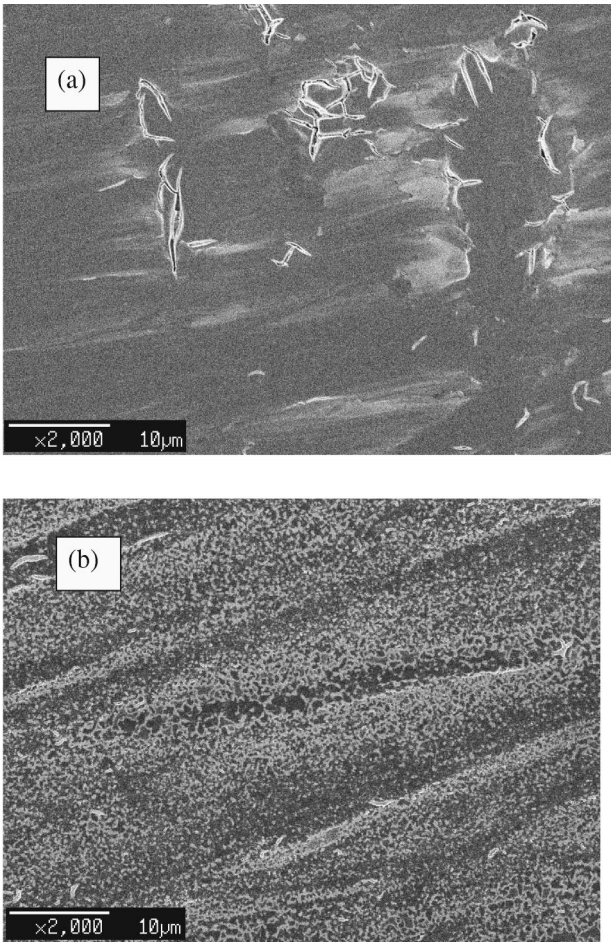

FIG. 7. FESEM micrographs: (a) sample S100 and (b) sample S800.

accurate thickness is not available, conclusions about the TiO_2 phase can be drawn from the experimental spectra.

Figure 8 shows the experimental spectra for the sol-gel films. We will use this set of samples to discuss the effect of the annealing temperature on the spectra and their relation to the crystallization process. For its shape and band position (875 cm^{-1}), the S100 spectrum is clearly associated to amorphous TiO_2, while the other three spectra are associated to the crystalline phases, having Berreman minima at 850 cm^{-1} (sample S400), 856 cm^{-1} (sample S600), and 813 cm^{-1} (sample S800). The difference between S400 and S600 spectra are the bandwidth, which is narrower for S600, and the minimum position. The band narrowing can be assigned to the fact that the crystallization process may be more advanced for an annealing temperature of 600 °C.

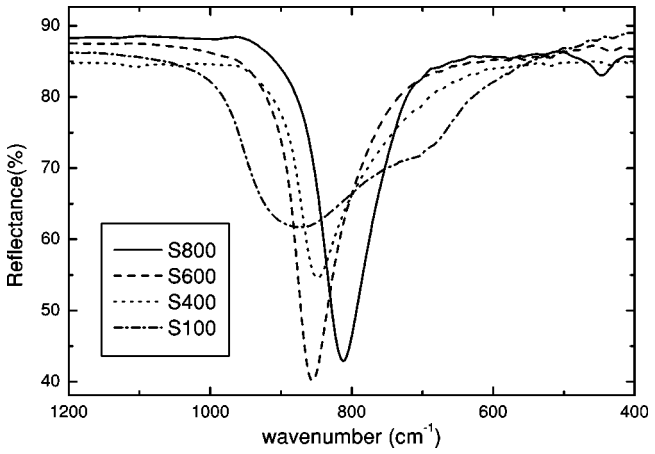

FIG. 8. Experimental spectra (p polarization and $\theta=70°$) for the sol-gel films (samples S100, S400, S600, and S800).

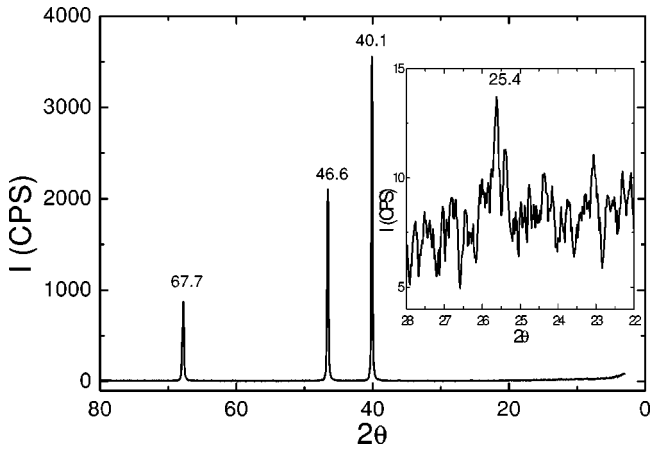

FIG. 9. X-ray diffractogram for samples S400. In the detail, the region within which the peak related to anatase should be observed.

According to our simulations, the differences between S600 and S800 spectra can be attributed to a phase change from anatase to rutile as the annealing temperature increased from 600 to 800 °C. The band observed at 447 cm^{-1} only for sample S800 corroborates our conclusion since it is related to an LO mode that is present only in the rutile LO function (Fig. 2). However, due to the fact that the most prominent band in the S800 spectrum extends from about 700 to 900 cm^{-1}, the possibility of a small quantity of anatase be present cannot be discarded.

X-ray diffraction was used to confirm our results. However, even the most intense peaks related to anatase and rutile,[43] at $2\theta=25.4°$ and $2\theta=27.5°$, respectively, are hardly discernible in the diffractogram, whereas the peaks associated to the platinum substrate are very clearcut (at $2\theta=39.7°$, $2\theta=46.2°$, and $2\theta=67.4°$). Figure 9 shows the diffractogram obtained for sample S400. While the peaks related to platinum are very prominent, the peak related to anatase is almost indiscernible due to noise. On the other hand, as shown in Fig. 8, a band with an intensity of about 30% (minimum at 850 cm^{-1}) can be observed in the infrared spectrum for sample S400.

IV. CONCLUSION

Profiting from Berreman effect, we have shown how infrared reflection-absorption can be used to characterize TiO_2 phases, even without knowledge of the exact film thickness. It is important to remark that in addition to crystalline

samples, it can also be used to characterize amorphous samples and films whose thickness does not allow the measurement of a reliable diffractogram. Furthermore, infrared reflection-absorption spectroscopy has advantages such as being a nondestructive, unexpensive and direct characterization technique.

ACKNOWLEDGMENTS

Financial support by the Fundação de Amparo à Pesquisa do Estado de São Paulo (Process 98/11743-2 and 95/9506-4) and the Conselho Nacional de Desenvolvimento Científico e Tecnológico are gratefully acknowledged.

*Corresponding author. e-mail: celso@iqm.unicamp.br

[1] R. Greenler, J. Chem. Phys. **44**, 310 (1966).
[2] K. Yamamoto and H. Ishida, Vib. Spectrosc. **8**, 1 (1994).
[3] A. Parikh and D. Allara, J. Chem. Phys. **96**, 927 (1992).
[4] T. Scherubl and L. Thomas, Appl. Spectrosc. **51**, 844 (1997).
[5] B. Harbecke, B. Heinz, and P. Grosse, Appl. Phys. A: Solids Surf. **38**, 263 (1985).
[6] D. Berreman, Phys. Rev. **132**, 2193 (1963).
[7] W.T. Paulewicz, G.J. Exarhos, W.E. Conaway, Appl. Opt. **22**, 1837 (1983).
[8] G.J. Exarhos, J. Vac. Sci. Technol. A **4**, 2962 (1986).
[9] D.M. Friedrich and G.J. Exarhos, Thin Solid Films **154**, 257 (1987).
[10] G.J. Exarhos, N.J. Hess, Thin Solid Films **220**, 254 (1992).
[11] D. Bahnemann, D. Bockelmann, and R. Goslich, Sol. Energy Mater. **24**, 564 (1991).
[12] B. Kraeutler and J. Bard, J. Am. Chem. Soc. **9**, 7729 (1977).
[13] J. Livage, M. Henry, and C. Sanchez, Prog. Solid State Chem. **18**, 259 (1988).
[14] M. Labavi, S. Doeuff, C. Sanchez, and J. Livage, Mater. Sci. Eng., B **3**, 203 (1989).
[15] W.G. Spitzer, R.C. Miller, D.A. Kleiman, and L.E. Howarth, Phys. Rev. **126**, 1710 (1962).
[16] D.M. Eagles, J. Phys. Chem. Solids **25**, 1243 (1964).
[17] S.P.S. Porto, P.A. Fleury, and T.C. Damen, Phys. Rev. **154**, 522 (1967).
[18] N.C. da Cruz, E.C. Rangel, J. Wang, B.C. Trasferetti, C.U. Davanzo S.G.C. Castro, and M.A.B. de Moraes, Surf. Coat. Technol. **126**, 123 (2000).
[19] K. Yamamoto and A. Masui, Appl. Spectrosc. **49**, 639 (1995).
[20] V. Hopfe, P. Bussemer, E. Richter, and P. Klobes, J. Phys. D **25**, 288 (1992).
[21] R.J. Gonzalez, R. Zallen, and H. Berger, Phys. Rev. B **55**, 7014 (1997).
[22] F. Gervais and B. Piriou, Phys. Rev. B **10**, 1642 (1974).
[23] M. Fujii, M. Wada, S. Hayashi, and K. Yamamoto, Phys. Rev. B **46**, 15 930 (1992).
[24] J. Sturm, P. Grosse, and W. Theiss, Z. Phys. B: Condens. Matter **83**, 361 (1991).
[25] V. Hopfe, E.H. Korte, P. Klobes, and W. Grahlert, Appl. Spectrosc. **47**, 423 (1993).
[26] M.F. MacMillan and R.P. Devaty, Phys. Rev. B **43**, 13 838 (1991).
[27] D.A.G. Bruggeman, Ann. Phys. (Leipzig) **24**, 636 (1939).
[28] J.C. Maxwell-Garnett, Philos. Trans. R. Soc. London, Ser. A **203**, 358 (1904).
[29] O. Hunderi, Phys. Rev. B **6**, 3419 (1973).
[30] C.G. Grandquist and O. Hunderi, Phys. Rev. B **18**, 2897 (1978).
[31] R.M. Almeida, Phys. Rev. B **45**, 0161 (1992).
[32] B.C. Trasferetti and C.U. Davanzo, Appl. Spectrosc. **54**, 502 (2000).
[33] B.C. Trasferetti, C.U. Davanzo, N.C. da Cruz, and M.A.B. de Moraes, Appl. Spectrosc. **54**, 687 (2000).
[34] A. Lehmann, Phys. Status Solidi B **148**, 401 (1988).
[35] A. Brunet-Bruneau, S. Fisson, G. Vuye, and J. Rivory, J. Appl. Phys. **87**, 7303 (2000).
[36] E.I. Kamitsos, A.P. Patsis, and G. Kordas, Phys. Rev. B **48**, 12 499 (1993).
[37] C.T. Kirk, Phys. Rev. B **38**, 1255 (1988).
[38] M.A. Ovchinnikov and C.A. Wight, J. Chem. Phys. **99**, 3374 (1993).
[39] M.A. Ovchinnikov and C.A. Wight, J. Chem. Phys. **100**, 972 (1994).
[40] M.A. Ovchinnikov and C.A. Wight, J. Chem. Phys. **102**, 67 (1995).
[41] M.A. Ovchinnikov and C.A. Wight, J. Chem. Phys. **103**, 9563 (1995).
[42] D. Palik, *Handbook of Optical Constants of Solids* (Academic Press, New York, 1985).
[43] J. Ragai and W. Lofti, Colloids Surface **61**, 97 (1991).